ELSEVIER

Journal of Power Sources 114 (2003) 121–126

JOURNAL OF POWER SOURCES

www.elsevier.com/locate/jpowsour

Improving low-temperature performance of Li-alloy anodes by optimization of the electrolyte–electrode interface

Xiang-Wu Zhang *, Chunsheng Wang, A. John Appleby

Center for Electrochemical Systems and Hydrogen Research, Texas Engineering Experiment Station, Texas A&M University, 238 Wisenbaker, College Station, TX 77843-3402, USA

Received 17 September 2002; accepted 27 September 2002

Abstract

The −20 °C performance of nano-tin-(lithium emeraldine base), i.e. nano-tin-(lithium hemi-oxidized polyaniline), abbreviated as nano-Sn-PAni, anodes was investigated. The rate-limiting process is slow charge-transfer kinetics, rather than poor electrolyte conductivity or a high solid electrolyte interface (SEI) film resistance. Two ionic conductors, i.e. Li^+-doped polyethylene oxide (PEO) and $14Li_2O–9Al_2O_3–38TiO_2–39P_2O_5$ ($(LiAlTiP)_xO_y$) ceramic powders were incorporated into the anode material to accelerate the interfacial charge-transfer process. The $(LiAlTiP)_xO_y$ ceramic proved to be much better than doped PEO in improving the low-temperature performance. One nano-Sn-PAni anode material containing 15 wt.% $(LiAlTiP)_xO_y$ gave particularly high initial charge and discharge capacities (795 and 545 mAh g^{-1}, respectively) at −20 °C.

Keywords: Low-temperature performance; Nano-tin; Polyaniline; Polyethylene oxide; Charge-transfer; Electronic-ionic mixed conduction

1. Introduction

Lithium-ion secondary cells have high energy density at moderate temperatures, and are now used in portable electronic equipment such as cellular telephones and lap-top computers [1]. However, their poor low-temperature performance makes them unsuitable for military and aerospace applications requiring operation at temperatures well below 0 °C. Recent papers have therefore focused on the low-temperature performance of Li-ion batteries [2–9]. Most previous studies suggest that poor Li-ion cell performance at low-temperatures is due to the electrolyte conductivity, which determines Li-ion mobility between the electrodes [2–5]. Various low-temperature electrolytes with low freezing points and high conductivities have been developed. However, recent results show that the primary cause of the poor low-temperature performance is related to electrode activity, which may be attributed to a combination of poor Li^+ ion transport at the solid electrolyte interphase (SEI), a high charge-transfer resistance, and/or slow Li diffusivity into the anode material [6–9]. Controversy still exists on the dominant low-temperature rate-controlling mechanism or mechanisms.

All published information on the low-temperature performance of Li-ion batteries is for those using carbon-based anodes. However, Li-alloys have been studied as possible replacements for carbonaceous anodes because of their much higher lithium atom packing density during Li insertion [10]. No information about the low-temperature performance of Li-alloy anodes has been published although the high electrochemical capacities of these anodes at room temperature have been widely reported [11–13].

In the present work, the low-temperature (−20 °C) performance of nano-tin-(lithium emeraldine base), i.e. nano-tin-(lithium hemi-oxidized polyaniline), code-named nano-Sn-PAni, anodes was investigated. Anodes with tin as host intercalation material have a theoretical capacity of 990 mAh g^{-1} [14]. The reason for using Li^+-doped PAni instead of the usual carbon black (CB) filled polyvinylidene fluoride (PVDF) binder is because it is an excellent stable electronic conductor after doping emeradine base with Li^+ ion from a lithium salt (sometimes incorrectly called pseudoprotonation). The doping mechanism has been described elsewhere [15–20]. The doped material can therefore simultaneously serve as an electronic conductor and a binder. A previous study showed that doped emeraldine salt PAni has a uniform electronic and morphological structure, which not only simplifies the electrolyte–electrode interface structure, but also provides good electrochemical anode performance

* Corresponding author. Tel.: +1-979-845-8281; fax: +1-979-845-9287.
E-mail address: xwzhang@tamu.edu (X.-W. Zhang).

0378-7753/02/$ – see front matter
PII: S0378-7753(02)00544-X

[21]. The low-temperature rate-controlling mechanism of nano-Sn-PAni anodes was studied using electrochemical impedance spectroscopy (EIS). To improve low-temperature performance, both organic and inorganic ionic conductors, namely, Li^+-doped polyethylene oxide (PEO) and $14Li_2O$–$9Al_2O_3$–$38TiO_2$–$39P_2O_5$ ($(LiAlTiP)_xO_y$) ceramic powders, were introduced to adjust the electrolyte–electrode interfacial state.

2. Experimental

2.1. Electrode preparation

Nano-Sn power (Argonide Corporation, Sanford, FL) of 98 nm mean particle diameter was used as the active material. The polymer binder used was emeraldine base PAni (EB, Aldrich Chemical, Milwaukee, WI) of molecular weight (M_W) 20,000 Da, which was doped (see below) with lithium hexafluorophosphate ($LiPF_6$, Aldrich Chemical) to give the corresponding emeraldine salt (ES), an excellent electronic conductor (2.9 S cm^{-1} with one Li^+ per two aniline units). The ionic conductors used to adjust the electrolyte–electrode interfacial state were Li^+-doped PEO (Aldrich Chemical, M_W 600,000 Da) and $14Li_2O$–$9Al_2O_3$–$38TiO_2$–$39P_2O_5$ ceramic powder. Doping of PEO took place simultaneously with that of PAni during anode preparation (see below). The $14Li_2O$–$9Al_2O_3$–$38TiO_2$–$39P_2O_5$ was prepared by he method described by Fu [22,23] from Li_2CO_3, $Al(OH)_3$, TiO_2, and $NH_4H_2PO_4$ starting materials [22,23]. The product was ball milled for 24 h and then sieved through a No. 325 mesh (≤45 μm).

The nano-Sn powder, PAni and $LiPF_6$ were added into 1-methyl-2-pyrrolidone (NMP) simultaneously. The mixtures were then stirred for 30 min, and cast directly onto the copper gauze to form the anodes, which were slowly-dried at room temperature overnight, followed by drying in vacuo at 75 °C for 24 h. The slowly-dried anodes have homogeneous and compact structures on the micrometer scale [21]. The anodes containing PEO or $(LiAlTiP)_xO_y$ were similarly prepared.

The active material content of all anodes was fixed at 70 wt.%. The area and thickness of the anodes as prepared were 1.0 cm^2 and 200–250 μm, respectively.

2.2. Electrochemical measurement

Electrochemical measurements were conducted in a three-electrode polytetrafluoroethylene (PTFE) cell. Two lithium foils were used as counter and reference electrodes. The electrolyte used for low-temperature work was 1.0 M $LiPF_6$ in 3:5:4:1 by volume ethylene carbonate (EC)–diethyl carbonate (DEC)–dimethyl carbonate (DMC)–ethyl methyl carbonate (EMC) mixture (Em Industries Inc.) [9]. To examine whether the electrolyte freezes at low-temperatures, a sample was sealed in a glass tube in the glove box, then exposed for 7 days at −20 °C, then at −30 °C. The electrolyte was found to remain completely liquid at these two temperatures.

Electrochemical cells were assembled in an argon-filled glove box. Charge (lithium insertion) and discharge (lithium extraction) was controlled by an Arbin (College Station, TX) automatic battery cycler at differing current densities with cut-off potentials of 0.05 and 1.2 V.

Electrochemical impedance spectroscopy (EIS) was performed using a Solarton FRA 1250 frequency response analyzer and a Solartron model 1286 electrochemical interface. Before each measurement, the electrodes were left on open-circuit for 5.0 h to allow their potential to stabilize. EIS measurements were then carried out using a 5.0 mV ac voltage signal in the 65 kHz–10 mHz frequency range in automatic sweep mode from high to low frequency.

3. Results and discussion

3.1. Low-temperature performance of nano-Sn-PAni anodes

Fig. 1 shows the potential profiles of the nano-Sn-PAni anode during the first charge–discharge cycle at 25 and −20 °C at current densities of 5 mA g^{-1}. At 25 °C, potential plateaus for Li insertion/extraction to and from nano-Sn particles appear during both charge and discharge. The initial (first cycle) charge and discharge capacities of the nano-Sn-PAni anode were 790 and 316 mAh g^{-1} at this temperature. However, when the temperature was decreased to −20 °C, high polarization was observed, making charging impossible.

The effects of high polarization can often be reduced by decreasing the charge–discharge current density.

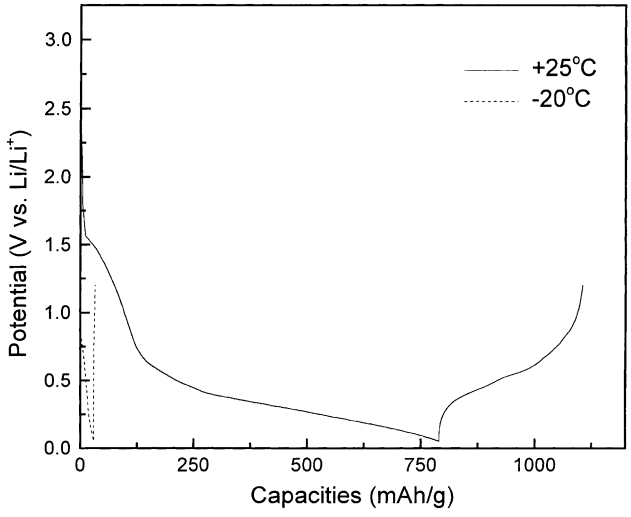

Fig. 1. Charge–discharge curves for nano-Sn-PAni anodes at 25 and −20 °C at 5 mA g^{-1} current density. The capacities are given with respect to the mass of active materials in the anodes.

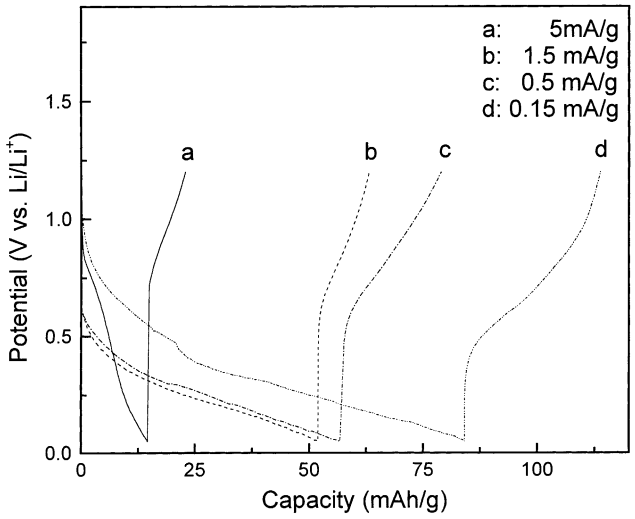

Fig. 2. Charge–discharge curves for nano-Sn-PAni anodes as a function of current density at −20 °C. Capacities as in Fig. 1.

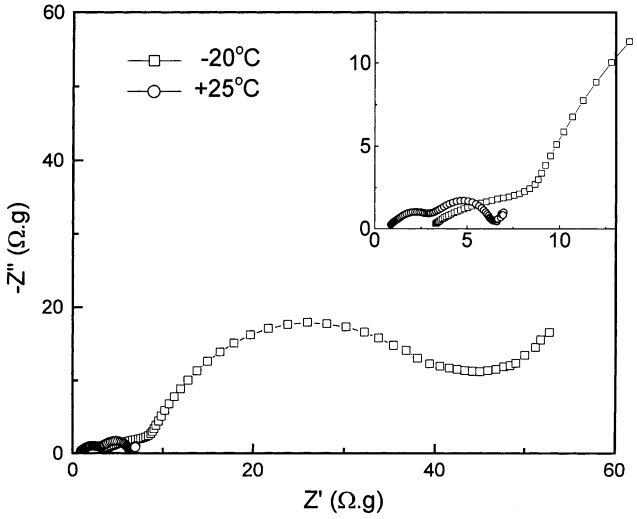

Fig. 3. Electrochemical impedance spectra of nano-Sn-PAni anodes at 25 and −20 °C. Before measurements, the anodes were left on open-circuit for 5.0 h.

Charge–discharge results (Fig. 2) were therefore obtained on the same nano-Sn-PAni anode at successively decreasing current densities at −20 °C. The polarization at this temperature was indeed strongly reduced by decreasing the current density. However, capacities were still very low (<100 mAh g^{-1}) even at the lowest current density examined (0.15 mAh g^{-1}). Some other effective approach must therefore be used to improve low-temperature performance, which first required a determination of the capacity-limiting process.

The cause of poor low-temperature carbon-based anode performance has been proposed as due to the low electrolyte conductivity, poor Li transport through the SEI film, high charge-transfer resistance, or low Li diffusivity into the active material. To determine the low-temperature rate-controlling mechanism, the impedance spectra of nano-Sn-PAni anode (Fig. 3) were obtained at different temperatures. Typical impedances in Fig. 3 show two separate depressed semicircles in the high-frequency range, with a linear portion at low frequencies. In general, the depressed semicircle at high frequencies is believed to be due to the impedance of the SEI film, and the second semicircle at middle frequencies is attributed to the interfacial lithium charge-transfer process [7,24–26]. The intersection of high-frequency line with the real axis is the electrolyte resistance between the working electrode and reference electrode. The linear portion at low frequencies is characteristic of Li diffusion in active intercalation materials. Fig. 3 shows that the electrolyte, SEI film and charge-transfer impedances all increase when the temperature is decreased from 25 to −20 °C. However, no detailed information about Li diffusion can be obtained from Fig. 3 because of the noise present in the sloping line data at low frequency.

The Fig. 3 data were analyzed using an equivalent circuit consisting a series resistance (the real part of the electrolyte resistance) and two parallel resistance capacitance circuits (the SEI film and interfacial charge-transfer impedance) [3,27,28]. The parameters in the equivalent circuit were calculated using the code Z_{view} (Version 1.4, Scribner Associates Inc.). The results show that the electrolyte, charge-transfer, and SEI film resistances (R_{el}, R_{ct}, and R_{SEI}, respectively) of the nano-Sn-PAni anode at 25 °C were 1.2, 2.5 and 3.1 Ω g, which increased to 3.3, 10.5 and 36.0 at −20 °C. The ratio of each element of resistance at the two temperatures in increasing order is $R_{el}\,(2.75) < R_{SEI}\,(4.20) < R_{ct}\,(11.61)$. The charge-transfer process has both the highest individual resistance at both temperatures and the largest temperature-dependent resistance ratio. Hence slow charge-transfer, rather than low electrolyte conductivity or a high SEI film resistance is the main cause of the poor low-temperature performance of nano-Sn-PAni anodes.

The charge-transfer process must always occur at the interface between the electronically conducting phase (electrode material) and the ionically conducting phase (electrolyte). Our previous work shows that the nano-Sn particles in the anodes studied are coated by the electronically conducting PAni emeraldine salt [21], therefore, the electronically conducting PAni film on active material surface obstructs charge-transfer since it cannot be a host to lithium. The introduction of an ionically conducting phase bridging the active material and the liquid electrolyte may accelerate the charge-transfer process, and thus improve low-temperature performance. Thus, the organic and inorganic ionic conductors Li^+-doped PEO and $(LiAlTiP)_xO_y$ were examined as bridging materials.

3.2. Low-temperature performance of nano-Sn-PAni-PEO anodes

PEO-lithium salt (LiX) complexes (abbreviated as doped PEO) are suitable polymer electrolytes for Li-ion batteries

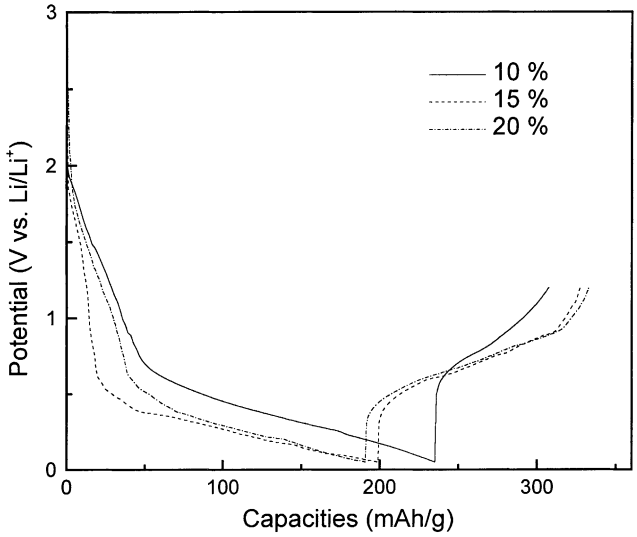

Fig. 4. Charge–discharge curves for nano-Sn-PAni-PEO anodes with various PEO contents at −20 °C and 0.5 mA g^{-1} current density. Capacities as in Fig. 1.

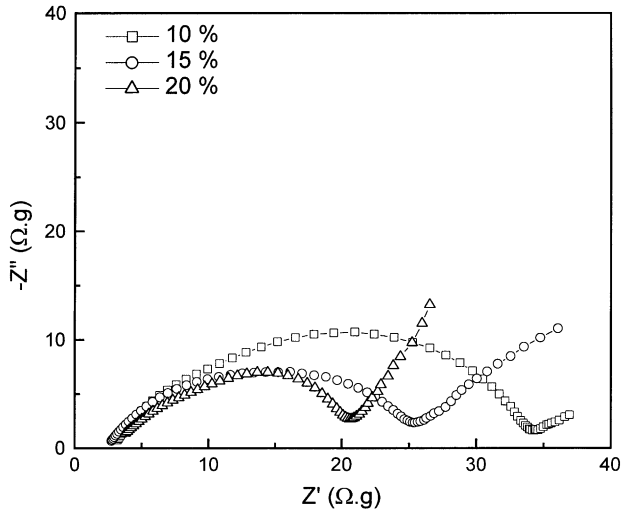

Fig. 5. Electrochemical impedance spectra of nano-Sn-PAni-PEO anodes as a function of PEO content at −20 °C.

[29]. The electrolyte uses the PEO chain ether groups in three-dimensional arrays to solvate Li^+ cations chains, with locally contiguous counterions for electroneutrality [30]. Doped PEO was used here to promote the interfacial process by forming ionically conducting bridges from the active materials to liquid electrolyte. Fig. 4 shows the potential profiles of the nano-Sn-PAni-PEO with differing PEO contents at −20 °C at a current density of 0.5 mA g^{-1}. As expected, the capacities of nano-Sn-PAni-PEO anodes (Fig. 4) are higher than those of nano-Sn-PAni anodes (Figs. 1 and 2), which confirms that the introduction of doped PEO indeed improves low-temperature performance. The doped PEO content of the anodes also influences the charge–discharge behavior. The initial charge capacities decrease from 235 to 198, 191 mAh g^{-1} as PEO content goes from 10 to 15, 20 wt.%, but the discharge capacities correspondingly increase from 72 to 129, 142 mAh g^{-1} The different capacity behavior for charge and discharge may be due to different kinetics, but they suggest that the presence of PEO inhibits SEI film formation.

Fig. 5 shows the impedance spectra of nano-Sn-PAni-PEO anodes at −20 °C. The two separate depressed semicircles merge into a single depressed semicircle, which is related to the different influence of doped PEO on the SEI film and on charge-transfer. The data in Fig. 5 were analyzed as in Fig. 3 and the resistance parameters calculated. The electrolyte resistances are around 3.0−4.0 Ω g, similar to the electrolyte resistance of the nano-Sn-PAni anode at −20 °C (3.3 Ω g). The small changes in electrolyte resistance may be attributed to differences in anode surface area and anode to reference electrode distance. Therefore, improvement in low-temperature performance seen in nano-Sn-PAni-PEO anodes must result from changes in the interfacial processes. When the PEO anode content goes from 0, 10, 15 to 20 wt.%, the SEI film resistances slightly decrease from 10.5, 10.4, 9.5, to 8.8 Ω g. However, the charge-transfer resistances decrease greatly from 36.0, 24.1, 14.3, to 12.2 Ω g. The active materials (nano-Sn) are the same in both anodes, so the introduction of doped PEO cannot change Li diffusivity. It can hence be concluded now that the doped PEO improve the low-temperature performance by accelerating the charge-transfer process at the electrolyte–electrode interface by increasing the available area of active material. The doped PEO therefore provides an ionically conducting phase between the active nano-Sn and liquid electrolyte. Part of the Li^+ cations can directly transfer through the doped PEO phase, which results in a decrease in charge-transfer resistance, giving improved low-temperature performance.

The appreciable intrinsic ionic conductivity of doped PEO (>10^{-4} S cm^{-1}) is only obtained at medium–high temperatures above the crystalline–amorphous transition temperature [29]. The conductivities of doped PEO are typically in the order of 10^{-6} to 10^{-8} S cm^{-1} at room temperature, and even less below 0 °C. Another disadvantage of doped PEO is its low Li^+ transference number (<0.2) [31], which further limits the effective conductivity of doped PEO during lithium charge-transfer. Therefore, the increase in the rate charge-transfer by doped PEO is limited, and the high discharge capacity of nano-Sn-PAni-PEO anodes is still less than 200 mAh g^{-1}. As a result, a more effective ionic conductor, i.e. $(LiAlTiP)_xO_y$, was examined.

3.3. Low-temperature performance of nano-Sn-PAni-$(LiAlTiP)_xO_y$ anodes

$(LiAlTiP)_xO_y$ ceramic is a solid electrolyte with the highest Li^+ ion conductivity known to date [22,23], and has a Li^+ transference number of unity [31]. It also retains high ionic conductivity at low-temperatures because of its low activity

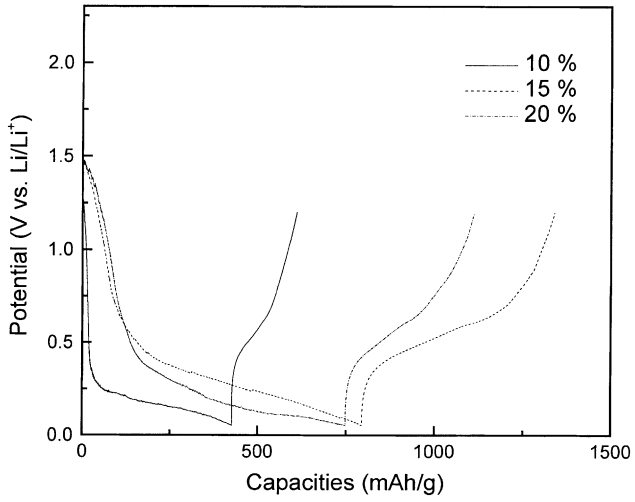

Fig. 6. Charge–discharge curves for nano-Sn-PAni-$(LiAlTiP)_xO_y$ anodes as a function of $(LiAlTiP)_xO_y$ content at −20 °C at 0.5 mA g^{-1} current density.

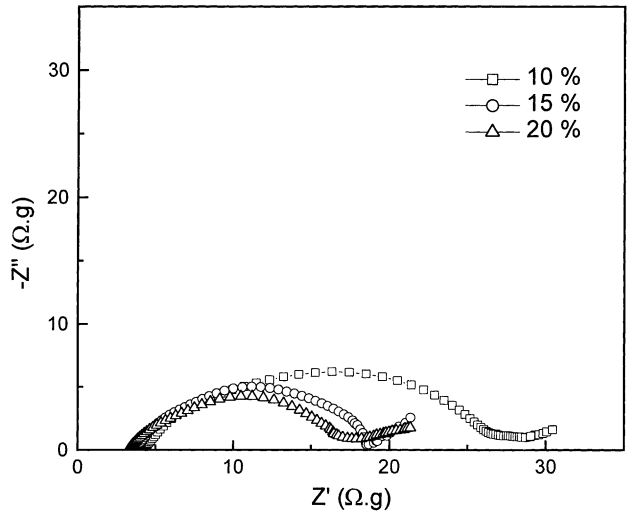

Fig. 8. Electrochemical impedance spectra of nano-Sn-PAni-$(LiAlTiP)_xO_y$ anodes as a function of $(LiAlTiP)_xO_y$ content at −20 °C.

energy for conduction (ca. 31.5 kJ mol^{-1}, [22]). The $(LiAlTiP)_xO_y$ composition synthesized for this work has a conductivity of 5×10^{-4} S cm^{-1} at 25 °C. Fig. 6 shows the potential profiles of the nano-Sn-PAni-$(LiAlTip)_xO_y$ anodes with differing $(LiAlTip)_xO_y$ contents at −20 °C at 0.5. On comparing Figs. 4 and 6, it is seen that the capacities are greatly improved by the addition of $(LiAlTiP)_xO_y$ ceramic powders. The anode containing 15 wt.% $(LiAlTiP)_xO_y$ had the highest charge and discharge capacities (795 and 545 mAh g^{-1}, respectively). Why capacity obtaimizes at this composition is presently unknown.

Nano-Sn-PAni anodes without additives show very high polarization at −20 °C and cannot be charged at a current density of 5 mA g^{-1} (Figs. 1 and 2). The potential profile of a nano-Sn-PAni-(15 wt.%) $(LiAlTiP)_xO_y$ anode at −20 °C was measured at 5 mA g^{-1} (Fig. 7). The nano-Sn-PAni-$(LiAlTiP)_xO_y$ anode has acceptable charge and discharge capacities (382 and 362 mAh g^{-1}, respectively) at this current density. Hence, $(LiAlTiP)_xO_y$ ceramic powder is a desirable ionic conducting additive to accelerate the interfacial process in Li-ion secondary cells operating at low-temperatures.

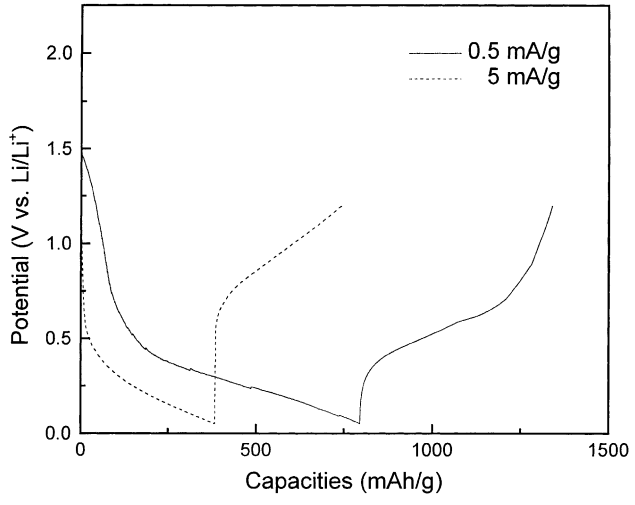

Fig. 7. Charge–discharge curves for nano-Sn-Pani-(15 wt.%) $(LiAlTiP)_xO_y$ anodes as a function of current density at −20 °C. Capacities as in Fig. 1.

Fig. 8 shows impedance spectra of nano-Sn-PAni-$(LiAlTiP)_xO_y$ anodes at −20 °C. The resistance parameters for the equivalent circuit were calculated as in Figs. 3 and 5. Again, the electrolyte resistances do not change greatly with changing $(LiAlTiP)_xO_y$ content. The SEI film resistances decrease only slightly from 10.5, 7.6, 7.3, to 6.0 Ω g when the $(LiAlTiP)_xO_y$ content is increased from 0, 10, 15, to 20%. However, the charge-transfer resistances greatly decrease from 36.0, 14.7, 8.8, to 7.8 with increasing $(LiAlTiP)_xO_y$ content. The high ionic conductivity and Li^+ transference number of $(LiAlTiP)_xO_y$ ceramic allows rapid Li^+ transfer between active material and liquid electrolyte, greatly improving the charge-transfer process and the low-temperature performance of the system studied.

4. Conclusions

The results of this work show that the poor low-temperature performance of lithium–tin alloy anodes largely result from their high charge-transfer resistance, not to a poorly-conducting electrolyte or solid electrolyte interface (SEI) film. The capacities of unmodified nano-Sn-PAni anodes are very low at −20 °C even at a very small current density (0.15 mA g^{-1}). This requires the development of new anode compositions to increase effective charge-transfer rates and improve capacities at low-temperatures.

The organic and inorganic ionic conductors Li^+-doped PEO and $(LiAlTiP)_xO_y$ ceramic powder have been examined as anode additives to provide ionically conducting bridges between the active materials and liquid electrolyte. Both can

decrease the charge-transfer resistance and thus increase the anode capacity. However, the $(LiAlTiP)_xO_y$ ceramic is superior in improving low-temperature performance because of its higher ionic conductivity.

Acknowledgements

We gratefully acknowledge NASA-Glenn Research Center (Grant No. NAG3-2617) for support of this work.

References

[1] J.M. Tarascon, M. Armand, Nature 414 (2001) 359.
[2] H.C. Shiao, D. Chua, H.P. Lin, S. Slane, M. Salomon, J. Power Sources 87 (2000) 167.
[3] M.C. Smart, B.V. Ratnakumar, S. Surampudi, Y. Wang, X. Zhang, S.G. Greenbaum, A. Hightower, C.C. Ahn, B. Fultz, J. Electrochem. Soc. 146 (1999) 3963.
[4] T. Nakajima, K.I. Dan, M. Koh, J. Fluor. Chem. 87 (1998) 221.
[5] E.J. Plichta, W.K. Behl, J. Power Sources 88 (2000) 192.
[6] F. Puglia, R. Gitzendanner, C. Marsh, T. Curran, J. Power Sources 96 (2001) 40.
[7] C.S. Wang, A.J. Appleby, F.E. Little, J. Electrochem. Soc., in press.
[8] H.P. Lin, D. Chua, M. Salomon, H.C. Shiao, M. Hendrickson, E. Plichta, S. Slane, Electrochem. Solid-State Lett. 4 (2001) A71.
[9] C.K. Huang, J.S. Sakamoto, J. Wolfenstine, S. Surampudi, J. Electrochem. Soc. 147 (2000) 2893.
[10] J.O. Besenhard, J. Yang, M. Winter, J. Power Sources 68 (1997) 87.
[11] O. Crosnier, X. Devaux, T. Brousse, P. Fragnaud, D.M. Schleich, J. Power Sources 97 (2001) 188.
[12] W.J. Weydanz, M. Wohlfahrt-Mehrens, R.A. Huggins, J. Power Sources 81 (1999) 237.
[13] M. Wachtler, J.O. Besenhard, M. Winter, J. Power Sources 94 (2001) 189.
[14] C.S. Wang, A.J. Appleby, F.E. Little, J. Power Sources 93 (2001) 174.
[15] A.V. Saprigin, K.R. Brenneman, W.P. Lee, S.M. Long, R.S. Kohlman, A.J. Epstein, Synth. Met. 100 (1999) 55.
[16] K.S. Ryu, B.W. Moon, J. Joo, S.H. Chang, Polymer 42 (2001) 9355.
[17] G. Min, Synth. Met. 119 (2001) 273.
[18] C.K. Jeong, J.H. Jung, B.H. Kim, S.Y. Lee, D.E. Lee, S.H. Jang, K.S. Ryu, J. Joo, Synth. Met. 117 (2001) 99.
[19] J. Joo, J.H. Jung, B.H. Kim, B.W. Moon, S.H. Chang, K.S. Ryu, Synth. Met. 119 (2001) 461.
[20] J.Y. Shimano, A.G. MacDiarmid, Synth. Met. 123 (2001) 251.
[21] X.W. Zhang, C.S. Wang, A.J. Appleby, F.B. Little, J. Power Sources, in press.
[22] J. Fu, Solid State Ionics 96 (1997) 195.
[23] J. Fu, J. Mater. Sci. 33 (1998) 1549.
[24] M. Dolle, F. Qrsini, A.S. Gozdz, J.M. Tarascon, J. Electrochem. Soc. 148 (2001) A851.
[25] C.C. Hu, C.H. Chu, J. Electroanal. Chem. 503 (2001) 105.
[26] F. Nobili, R. Tossici, F. Croce, B. Scrosati, R. Marassi, J. Power Sources 94 (2001) 238.
[27] J.G. Thevenin, R.H. Muller, J. Electrochem. Soc. 134 (1987) 273.
[28] M.W. Wagner, Electrochim. Acta 42 (1997) 1623.
[29] G.B. Appetecchi, W. Henderson, P. Villano, M. Berrettoni, S. Passerini, J. Electrochem. Soc. 148 (2001) A1171.
[30] P. Lightfoot, M.A. Metha, P.G. Bruce, Science 262 (1993) 883.
[31] K. Nairn, M. Forsyth, H. Every, M. Greville, D.R. MacFarlane, Solid State Ionics 86 (1996) 589.